Journal of Alloys and Compounds 695 (2017) 1213–1222

Contents lists available at ScienceDirect

Journal of Alloys and Compounds

journal homepage: http://www.elsevier.com/locate/jalcom

Effect of local environment on moment formation in iron silicides

N.G. Zamkova [a], V.S. Zhandun [a, *], S.G. Ovchinnikov [a, b], I.S. Sandalov [a]

[a] Kirensky Institute of Physics, Federal Research Center KSC SB RAS, Akademgorodok 50, 660036 Krasnoyarsk, Russia
[b] National Research Nuclear University MEPhI, Kashurskoe sh. 31, 115409 Moscow, Russia

ARTICLE INFO

Article history:
Received 11 July 2016
Received in revised form
4 October 2016
Accepted 10 October 2016
Available online 27 October 2016

Keywords:
Ab initio calculations
Multiorbital model
Iron silicides
Magnetic properties
Spin-crossover

ABSTRACT

The effect of local environment on the formation of magnetic moments on *Fe* atoms in iron silicides is studied by combination of *ab initio* and model calculations. The suggested model includes all *Fe d*- and *Si p*-orbitals, intra-atomic Coulomb interactions, inter-atomic *Fe-Fe* exchange and hopping of electrons to nearest and next nearest neighboring atoms. The parameters of the model are found from the requirement that *self-consistent* moments on atoms and density of states found from *ab initio* and model calculations within the Hartree-Fock approximation are close to each other as much as possible. Contrary to the commonly accepted statement that in the ordered Fe_3Si and Fe_xSi_{1-x} alloys an increase of the *Si* concentration within nearest environment of *Fe* atoms results in a decrease of *Fe* magnetic moment we find that a crucial role in the formation of magnetic moments is played by the second coordination sphere of *Fe* atoms. Particularly, the *Fe* atoms have higher magnetic moments in amorphous films compared to the epitaxial ones due to decreasing the number of iron-atoms in the next nearest environment. Both our model and *ab initio* calculations confirm existence of known spin crossover with pressure and predict second crossover at higher pressure.

1. Introduction

The transition metal silicides, particularly iron silicides, offer a large variety of potential spintronic, microelectronic and optoelectronic applications for silicon-based devices. Depending on their phase, crystal structure and composition, they can be semiconducting or metallic with different ferro- (FM), ferri- (FiM) or paramagnetic (PM) states. The binary Heusler alloy, Fe_3Si, is a potentially good candidate for a spin injector. This material has a high Curie temperature ($\approx$840 K) with theoretically predicted high spin-polarization [1–5]. At the *Fe*-rich side of the binary phase diagram, metallic as well as ferromagnetic Fe_5Si_3 and Fe_3Si have already been established as key materials for spintronics. The *Si*-rich side of the phase diagram [6] contains several variants of a disilicide stoichiometric compound, such as the high-temperature tetragonal metallic α-$FeSi_2$ phase, with applications as an electrode or an interconnect material, and the orthorhombic semiconducting β-$FeSi_2$ phase, which due to its direct band gap is an interesting candidate for thermoelectric and optoelectronic devices. One of the motivations for studying the $Fe - Si$ system is the possibility to tune its magnetic properties. The experiments [7,8] on bulk Fe_xSi_{1-x} alloys have revealed strong dependence of the magnetic properties on *Si* concentration and chemical order. The local magnetic moments at *Fe* sites may become higher than in pure iron, depending on the distribution of *Fe* and *Si* neighbors, and disappear at *Si* concentration close to 50%. The presence of the *Si* neighbors decreases the average magnetic moment at the *Fe* sites, resulting in the appearance of high- and low-spin *Fe* species. This has been established for ordered and disordered Fe_xSi_{1-x} by neutron diffraction [9,10], Mössbauer effect measurements [11,12] and pulsed NMR studies [13]. The iron silicides are also technologically advantageous since they can be grown epitaxially on many different semiconductor and insulator substrates [14–19]. What makes the system Fe_xSi_{1-x} unique is that it allows for varying the degrees of both chemical and structural order over a wide composition range with the thin film growth techniques; the high-quality epitaxial films on *Si* may exhibit ferromagnetism. The latter promises perspective for the integration of the *FeSi*-based magnetic devices into silicon technology. Furthermore, the iron silicides, which do not exist in bulk, can be stabilized as films. Recently a successful fabrication of thin films solid solution Fe_xSi_{1-x} within the composition range $0.5 < x < 0.75$ with the *CsCl* structure (B2) was reported [14,16]. Also, while the magnetic order is not observed in bulk stoichiometric disilicide $FeSi_2$, ferromagnetism was found [20]

* Corresponding author.
E-mail address: jvc@iph.krasn.ru (V.S. Zhandun).

http://dx.doi.org/10.1016/j.jallcom.2016.10.248
0925-8388/

in the metastable phase α-FeSi2, which was stabilized in epitaxial-film form on the silicon substrate.

Most of theoretical works were devoted to the solid solutions *Fe-Si* from *Fe*-rich side of the phase diagram with *bcc*-like structures (DO_3, B2, A2). The phenomenological models [11,21,22], have been suggested for the explanation of the measured hyperfine fields at *Fe* atoms with different numbers of *Fe* as first neighbors. The results obtained within the models are consistent with the experimentally observed linear decrease of the *Fe* moment with concentration of *Si* ions in first coordination sphere. The electronic structure and magnetic properties of the ordered bulk Fe_3Si and its solid solutions Fe_xSi_{1-x}, $Fe_{3-x}T_xSi$, where *T* is a transition metal, $Fe_{3-x}V_xX$ with $X = Si,Ga,Al$, have been studied by *ab initio* calculations [23–27]. The calculation of moments and electronic structure of binary Fe_xSi_{1-x} and ternary $Fe_{3-x}V_xSi$ random alloys with DO_3-like structure within coherent potential approximation (CPA) [23] has confirmed the conclusions of the phenomenological model about practically linear variation of the *Fe* magnetic moment with the number of nearest *Fe* neighbors. The same was stated in the later theoretical works within non-cluster CPA [24–27]. However, non-cluster CPA method is an effective-medium method by construction. This method as well as local environment models [11,21,22] provide information about influence of *only* average number of metallic or metalloid atoms on the magnetic moment formation. For this reason they are not able to reflect the role played by the different local environment at the same concentration of the alloy components. Furthermore as emphasized in the works [8,28] on Mössbauer spectra, the contribution of the second neighbors of *Fe* ions to the formation of its moment is far from being negligible. We found two theoretical attempts to attract attention to this problem [29,30]. In Ref. [29] the *d*-electrons were mimicked by Hubbard's *s*-band, hybridized with the *Si* single-band of non-interacting electrons. The dependence on the local environment was described via the position of *d*-level. The authors in Ref. [29] come to the conclusion that the local magnetic moment is determined by the number of metalloid atoms and weakly depends on its concentration. Due to oversimplification of the model it remains unclear, however, if these conclusions are related to the compounds of interest or not. More realistic model [30], which is close to our model, which we will use here, includes all five *3d*-electron orbitals of *Fe* and three *3p*-orbitals *Si*, and the Slater-Koster approach [31] for hopping integrals. The work [30] was devoted to the solution of the experimentally known puzzle: why the impurities from left side of Fe (say, Mn) prefer to occupy the cubic-symmetry sites, whereas those from right side (like Co) the tetrahedral-symmetry sites. The magnetism in this work was treated via the only Stoner's exchange-splitting parameter, which was used to fit the *average* magnetic moment to the experimental one. Unfortunately, the latter simplification does not allow to describe the effects of local environment in these compounds.

The target of this work is to investigate the influence of local environment on the formation of iron-atoms' magnetic moments in the iron silicides Fe_3Si and solid solutions Fe_xSi_{1-x}. Particularly, we will address the question, raised in the experimental works [8,28], about the role played by second neighbors of *Fe* ions. The dependence of the *Fe* moments on pressure and the possibility of the high-spin - low-spin crossover will be investigated also.

The paper is organized as follow. In Sec. 2 we formulate the multiorbital model and provide the details of *ab initio* calculations. In Sec. 3 the results of the model and *ab initio* calculations of Fe_3Si and its alloys are compared and the dependence of magnetic moments on the hopping matrix elements is presented. The spin-crossovers under pressure in Fe_3Si are described in Sec. 4. The formation of magnetic moments in the alloys Fe_xSi_{1-x} is considered in Sec. 5. Sec. 6 contains the summary of the obtained results and conclusions.

2. The approach

It is difficult to separate the contributions of the first and second neighbors to the magnetic moment formation on the *Fe* atoms in *ab initio* schemes. For this reason we combine the *ab initio* calculations with the model one. We use the following scheme. Firstly we have performed the calculation of electronic and magnetic properties of the compound of interest within the framework of density functional theory in the generalized gradient approximation (DFT-GGA) for the different substitutions of silicon atoms by the iron atoms. Then we perform mapping the DFT-GGA results to the model. The guiding arguments for the formulation of the model are: the model should 1) has a minimal number of parameters; 2) contain the specific information about the compound in question (*i.e.*, the proper number of orbitals and electrons and reflect the crystal structure) and 3) contain main interactions, reflecting our understanding of the underlying physics. At last, we perform the mapping following the DFT ideology: we find the parameters of the model from fitting *its self-consistent charge density* to the one, obtained by *ab initio* calculations. The latter step distinguishes our approach from the other ones.

2.1. The ab initio part

All *ab initio* calculations presented in this paper are performed using the Vienna *ab initio* simulation package (VASP) [32] with projector augmented wave (PAW) pseudopotentials [33]. The valence electron configurations $3d^64s^2$ are taken for *Fe* atoms and $3s^23p^2$ for *Si* atoms. The calculations are based on the density functional theory where the exchange-correlation functional is chosen within the Perdew-Burke-Ernzerhoff (PBE) parameterization [34] and the generalized gradient approximation (GGA) has been used. Throughout all calculations, the plane-wave cutoff energy 500 eV is used. The Brillouin-zone integration is performed on the grid Monkhorst-Pack [35] special points $10 \times 10 \times 10$.

2.2. The model part

One can conclude from the experiments [9–13] that the *d*-electrons in iron silicides are delocalized. At the same time there is a consensus in scientific community that the intraatomic interactions are strong enough to contribute to the formation of the *Fe* ions moment. We include into the Hamiltonian of our model the set of interactions between the *d*-electrons of *Fe (5 d*-orbitals per spin) following Kanamori [36]. The compounds under consideration contain neighboring *Fe* ions, therefore, the interatomic direct *d-d*-exchange and *d-d*-hopping cannot be ignored. The *Si p*-electrons (*3p*-orbitals per spin) are modeled by atomic levels and interatomic hoppings, no *p-p*-Coulomb terms are included. Both subsystems are connected by *d-p*-hoppings. Thus, the Hamiltonian of the model is:

$$H = H^{Fe} + H_{J'}^{Fe-Fe} + H_0^{Si} + H_{hop}, \;\; H^{Fe} = H_0^{Fe} + H_K^{Fe} \qquad (1)$$

where

$$H_0^{Fe} = \sum \varepsilon_0^{Fe} \hat{n}_{nm\sigma}^{d}; \; H_0^{Si} = \sum \varepsilon_0^{Si} \hat{n}_{nm\sigma}^{p};$$

and the Kanamori's part of the Hamiltonian

$$H_K^{Fe} = \frac{U}{2}\sum \hat{n}^d_{nm\sigma}\hat{n}^d_{nm\bar{\sigma}} + \left(U' - \frac{1}{2}J\right)\sum \hat{n}^d_{nm}\hat{n}^d_{nm'}(1-\delta_{mm'}) - \frac{1}{2}J\sum \hat{s}^d_{nm}\hat{s}^d_{nm'};$$

$$H_{J'}^{Fe-Fe} = -\frac{1}{2}J'\sum \hat{s}^d_{nm}\hat{s}^d_{n'm'};$$

$$\mathscr{H}_{hop} = \sum T^{mm'}_{nn'}p^\dagger_{nm\sigma}p_{n'm'\sigma} + \sum t^{mm'}_{nn'}d^\dagger_{nm\sigma}d_{n'm'\sigma} + \sum\left[(t')^{mm'}_{nn'}d^\dagger_{nm\sigma}p_{n'm'\sigma} + H.c.\right];$$

$$\hat{n}^d_{nm\sigma} \equiv d^\dagger_{nm\sigma}d_{nm\sigma};\ \hat{n}^d_{nm} = \hat{n}^d_{nm\uparrow} + \hat{n}^d_{nm\downarrow};\quad \hat{s}^d_{nm} \equiv \sigma_{\alpha\gamma}d^\dagger_{nm\alpha}d_{nm\gamma};\ \hat{n}^p_{nm\sigma} \equiv p^\dagger_{nm\sigma}p_{nm\sigma}. \tag{2}$$

Here and are the creation (annihilation) operators of *p*-electrons of *Si*- and *d*-electrons of *Fe*-ions; *n* is a complex index lattice (site, basis); *m* labels the orbital; σ is spin projector index; $\sigma_{\alpha\gamma}$ are Pauli matrices; $U, U' = U - 2J$ and J are the intra-atomic Kanamori parameters; J' is the parameter of the intersite exchange between nearest *Fe* atoms. At last, $T^{mm'}_{nn'}$, $t^{mm'}_{nn'}$, $(t')^{mm'}_{nn'}$ are hopping integrals between atoms *Si*-*Si*, *Fe*-*Fe* and *Fe*-S atoms, correspondingly. Notice that in order to reduce the number of parameters we did not include into Hamiltonian the terms, describing the crystal electric field. Therefore, in atomic limit (all $t = 0$) all iron-atoms' are completely identical. Since the hopping matrix elements fully reflect the crystal symmetry, they provide the splitting of the atomic states of *Fe* ions according to the symmetry of the local environment. They are fitting parameters of the model; for this reason we avoid to introduce additional crystal-field parameters.

Since our target is to obtain the zero-temperature phase diagram for magnetic moment formation and in present report we do not study the thermodynamics, it is sufficient to analyze the system within Hartree-Fock approximation (HFA) from weak-coupling side. After standard HFA decoupling and Fourier transformation we obtain the matrix equation for the Green's functions for each spin for spin-homogeneous states:

$$\left(E\delta_{ii_1}\delta_{mm_1} - \Omega^\sigma_{im,i_1m_1}(\boldsymbol{k})\right)G^\sigma_{i_1m_1,i'm'}(\boldsymbol{k},E) = \delta_{ii'}\delta_{mm'}, \tag{3}$$

where *m* stands for orbital and *I* labels atom in the basis. The matrix $\Omega^\sigma_{\Im,i_1m_1}$ consists of the blocks,

$$\Omega(k) = \begin{pmatrix} \Omega_{FeFe}(k) & \Omega_{FeSi}(k) \\ \Omega^\dagger_{FeSi}(k) & \Omega_{SiSi}(k) \end{pmatrix}, \tag{4}$$

that have the form

$$[\Omega_{FeFe}(\boldsymbol{k})]^\sigma_{\lambda i,\mu j} = \delta_{\lambda\mu}\delta_{ij}\varepsilon^{Fe}_{i\sigma} - t^{\lambda\mu}_{ij}(\boldsymbol{k}),\ \ [\Omega_{FeSi}(\boldsymbol{k})]^\sigma_{\lambda i,\mu j} = [t'(\boldsymbol{k})]^{\lambda\mu}_{ij}, \tag{5}$$

$$[\Omega_{SiSi}]^\sigma_{\lambda i,\mu j}(k) = \delta_{\lambda\mu}\delta_{ij}\varepsilon^{Si}_{i\sigma} - T^{\lambda\mu}_{ij}(\boldsymbol{k}) \tag{6}$$

with

$$\varepsilon^{Fe}_{i\sigma} = \varepsilon^{Fe}_0 + Un^{d,\bar{\sigma}}_{i\lambda} + U'\sum_{m\neq\lambda} n^d_{im} - 2J\eta(\sigma)\sum_m \sigma^{d,z}_{im} - 2J'\eta(\sigma)\sum_{l,m}\sigma^{d,z}_{lm} \tag{7}$$

$$n^{d,\bar{\sigma}}_{i\lambda} = \sum_k\left\langle d^\dagger_{k,i\lambda\bar{\sigma}}d_{k,i\lambda\bar{\sigma}}\right\rangle,\quad n^{d,\sigma}_{i\lambda} = \sum_k\left\langle d^\dagger_{k,i\lambda\sigma}d_{k,i\lambda\sigma}\right\rangle,\quad \sigma^{d,z}_{im} = \frac{1}{2}\sum_\sigma \sigma n^{d,\sigma}_{im}. \tag{8}$$

And $\eta(\uparrow) = 1, \eta(\downarrow) = -1$. Then the self-consistent equations for population numbers are expressed in terms of eigenvalues $\varepsilon^\sigma_\nu(\boldsymbol{k})$ and eigenvectors $u^{\nu\sigma}_{im}(\boldsymbol{k})$ of matrix $\Omega^\sigma_{im,i_1m_1}(\boldsymbol{k})$:

$$n^{d,\sigma}_{im}(\boldsymbol{k}) = \left\langle d^\dagger_{k,im\sigma}d_{k,im\sigma}\right\rangle = \sum_\nu\left[u^{\nu\sigma}_{im}(\boldsymbol{k})\right]^* f(\varepsilon^\sigma_\nu(\boldsymbol{k}) - \mu)u^{\nu\sigma}_{im}(\boldsymbol{k}). \tag{9}$$

Particularly, for the Fe_3Si the matrix $\widehat{\Omega}$ has size 18×18 for each spin. The function $f(x) = [1+exp(x/T)]^{-1}$ is the Fermi distribution function, chemical potential μ is found from the full number of electrons per the cell.

The dependences of hopping integrals $t^{mm'}_{nn'}$, $(t')^{mm'}_{nn'}$, $T^{mm'}_{nn'}$ on $\boldsymbol{k}$ were obtained from the Slater and Koster atomic orbital scheme [31] in the two-center approximation using basic set consisting of five 3*d* orbitals for each spin on each *Fe* and three 3*p* orbital for each spin on each *Si*. In this *two-center approximation* the hopping integrals depend on the distance $\boldsymbol{R} = (l\mathbf{x} + m\mathbf{y} + n\mathbf{z})$ between the two atoms, where **x, y, z** are the unit vectors along cubic axis and *l*, *m*, *n* are direction cosines. Then, within the two-center approximation, the hopping integrals are expressed in terms of Slater −Koster parameters $t_\sigma \equiv (dd\sigma)$, $t_\pi \equiv (dd\pi)$ and $t_\delta \equiv (dd\delta)$ for $Fe - Fe$ hopping and $t_\sigma \equiv (pd\sigma)$, $t_\pi \equiv (pd\pi)$ for *Fe*- *Si* and $Si - Si$ hoppings (σ, π, δ specifies the component of the angular momentum relative to the direction $\boldsymbol{R}$). Their $\boldsymbol{k}$-dependence are given by the functions $\gamma_\sigma(\boldsymbol{k})$, $\gamma_\pi(\boldsymbol{k})$ and $\gamma_\delta(\boldsymbol{k})$, where $\gamma(k) = \sum_R e^{ikR}$. The expressions for hopping integrals can be obtained from Table 1 [31]. For example, $t^{xy,xy}_{Fe-Fe}(\mathbf{k}) = 2t_\pi(\cos(R_xk_x) + \cos(R_yk_y)) + 2t_\delta cos(R_zk_z)$, *etc.*

The population numbers $n^{d,\sigma}_{im}(\boldsymbol{k})$, $n^{p,\sigma}_{im}(\boldsymbol{k})$ have been found self-consistently with the accuracy *o* (10^{-3}). The number of points in the Brillouin zone for the *FCC* lattice was taken 512 and 1000 for the *SC* lattice. The Monkhorst-Pack scheme [35] was used for generation of the k-mesh. The calculations were performed from three initial states: *FM*, *AFM* and *PM* states. After achieving self-consistency the state with minimal total energy was chosen. The last step was done with the help of the Galitsky-Migdal formula for total energy, which we adopted for our model. Within HFA it acquires the form:

$$E_{tot} = \frac{1}{2}\sum_{ij\lambda\mu}\sum_{\nu k}\left[u^{\nu\sigma}_{im}(\boldsymbol{k})\right]^*\left(\tau^{\lambda\mu}_{ij}(\boldsymbol{k}) + \varepsilon^\sigma_\nu(\boldsymbol{k})\right)f(\varepsilon^\sigma_\nu(\boldsymbol{k}) - \mu)u^{\nu\sigma}_{im}(\boldsymbol{k}), \tag{10}$$

with

$$\tau^{\lambda\mu}_{ij}(\boldsymbol{k}) = \delta_{ij}\delta_{\lambda\mu}\varepsilon^0_i + t^{\lambda\mu}_{ij}(\boldsymbol{k}) + (t')^{\lambda\mu}_{ij}(\boldsymbol{k}) + T^{\lambda\mu}_{ij}(\boldsymbol{k}) \tag{11}$$

(we remind that the basis indices *i*,*j* label the sorts of atoms).

3. The dependence of moments on hopping

Stoichiometric Fe_3Si has the DO_3 crystal structure with the space symmetry group $Fm3'm$ and with four atoms in the unit cell (Fig. 1a). The iron-atoms' have two nonequivalent crystallographic positions Fe_I and Fe_{II}. Fe_I and *Si* sit in the cubic positions with the point-group symmetry O_h, whereas Fe_{II} are in the tetrahedral

Table 1
The comparison of the model and GGA-DFT orbital populations ($n^d_\uparrow$, $n^d_\downarrow$), magnetic moments (μ) and the number of electrons (N_{el}). The last column contains hopping parameters providing the best fit.

	Orbital	VASP				Model				Hopping parameters
		$n^d_\uparrow$	$n^d_\downarrow$	μ, μ_B	N_{el}	$n^d_\uparrow$	$n^d_\downarrow$	μ, μ_B	N_{el}	
Fe_I	t_{2g}	0.84	0.51	2.52	6.2	0.82	0.43	2.55	6.1	$t_{1\sigma} = 0.55$ $t_{1\pi} = t_{1\sigma}/3 = 0.187$
	e_g	0.92	0.18			0.94	0.25			$t_{2\sigma} = 1.0$ $t_{2\pi} = t_{2\sigma}/2 = 0.5$
Fe_{II}	t_{2g}	0.79	0.57	1.32	6.4	0.79	0.53	1.35	6.5	$t_{3\sigma} = 0.4$ $t_{3\pi} = t_{3\sigma}/2 = 0.2$
	e_g	0.77	0.38			0.78	0.49			$t_{4\sigma} = 0.7$ $t_{4\pi} = t_{4\sigma}/2 = 0.35$
										$t_{5\sigma} = 0.8$ $t_{5\pi} = t_{5\sigma}/2 = 0.4$

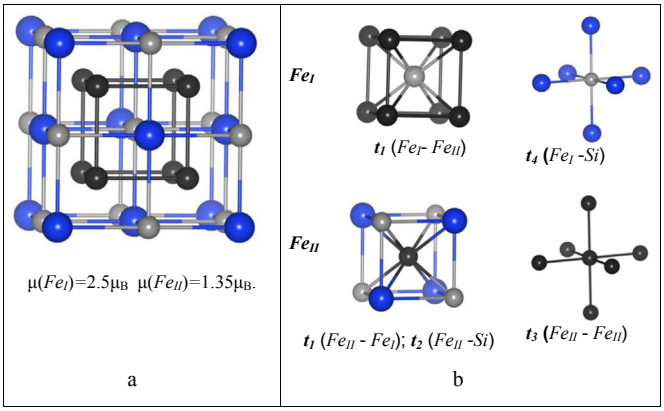

Fig. 1. (a) The structure of Fe_3Si: Fe_I is grey, Fe_{II} is black; (b) Nearest and next-nearest neighbors of Fe_I and Fe_{II} atoms along with the model hopping parameters.

positions with the symmetry T_d. Inequivalent *Fe* ions have different local environment in both first (NN) and second coordination spheres (NNN). Fe_I is surrounded by eight Fe_{II} in NN and six *Si* atoms in NNN. Nearest environment of Fe_{II} contains four Fe_I atoms and four *Si*, while next-nearest environment of Fe_{II} consists of six Fe_{II} atoms. Such a different distribution of *Si* neighbors results in very different magnetic moments μ on *Fe* ions: $\mu(Fe_I) = 2.5\mu_B$ and $\mu(Fe_{II}) = 1.35\mu_B$ [21,23].

All *ab initio* calculations of the density of electronic states (DOS) and magnetic moments have been performed with the equilibrium lattice parameters, which are found from the full optimization of the structure geometries within GGA. For the Fe_3Si in DO_3-type of structure we have obtained $a = 5.60$ Å. The distance between nearest neighbors are $R_{NN} = 2.42$ Å and between next-nearest ones are $R_{NNN} = 2.80$ Å. The distance between nearest *Si* atoms is $R_{Si-Si} = a\frac{\sqrt{2}}{2}$.

In model calculations all parameters were taken in the units of *U*. We used the following parameters: $J = 0.4$, $J' = 0.05$, $\varepsilon^{Si} = 6$, $\varepsilon^{Fe} = 0$. There are five hopping parameters for the Fe_3Si: t_1 and t_2 between NN, where $t_1 \equiv t$ ($R_{FeI-FeII}$) for Fe_I - Fe_{II} neighbors and $t_2 \equiv t$ ($R_{FeII-Si}$) for $Fe_{II} - Si$ ones; t_3, t_4 between NNN, where $t_3 \equiv t$ ($R_{FeII-FeII}$) for Fe_{II}- Fe_{II} neighbors and $t_4 \equiv t$ (R_{FeI-Si}) for $Fe_I - Si$ ones; and $t_5 \equiv t$ (R_{Si-Si}) for Si −Si neighbors. In order to decrease the number of parameters, the weak δ-bonds are neglected ($t_{1\delta} = t_{3\delta} = 0$).

The values of the parameters are found from the requirement that after achieving self-consistency in both the model (HFA) and in *ab initio* calculations (GGA), the *d*-DOS and magnetic moments on *Fe* atoms have to be as close to each other as possible. The comparison of the model and GGA *Fe d*-population numbers are shown in Table 1 at the parameters from the last column of Table 1. As can be seen, these parameters provide small enough error in occupations of the orbitals to convince that the model reflects the properties of real compounds.

The corresponding partial DOS (pDOS) are compared in Fig. 2. As seen, qualitatively the peculiarities of *d*-pDOS for inequivalent *Fe* atoms, like well pronounced peaks for Fe_I and smeared pDOS for Fe_{II}, are reproduced by the model. However, the model pDOS occupies narrower interval of energy and is concentrated in the region closer to Fermi energy. As mentioned above, we assume that this is due to absence of *s*-, *p*-electrons of *Fe* and *s*-electrons of *Si* in the model.

The relation between t_σ and t_π shown in Table 1 was kept in all model calculations, for this reason we will use notation $t_\sigma \equiv t$ further everywhere.

Let us consider firstly the scenario of the magnetic moment formation on *Fe* ions suggested in earlier models [11,21,22] and CPA [23] calculations for Fe_3Si where magnetic moments are fully determined by the nearest environment. In our model this corresponds to the switch off the hopping integrals between second neighbors' t_3 and t_4. Corresponding *Fe*-moment dependences on the NN hopping constants t_1 and t_2 at NNN hoppings $t_3 = t_4 = 0$ is shown in Fig. 3a. In this limit, the ferromagnetic solution exists at any considered values t_1, t_2. The magnetic moments at both types of *Fe* ions weakly depend on the hopping parameter t_2 between NN Fe_{II} - *Si* being determined mainly by the hopping parameter t_1 between NN Fe_I -Fe_{II}. The dependence of the moment $\mu_{FeI}(t_1)$ on the hopping parameter t_1 is sharper than $\mu_{FeII}(t_1)$. Particularly, the moment $\mu_{FeI}(t_1)$ drops quite fast to zero near the line $|t_1| \approx 0.7$, whereas $\mu_{FeII}(t_1)$ dependence remains smooth. It is important that if the hoppings between NNN are absent there is no region where the values of magnetic moments on both Fe_I and Fe_{II} atoms are close to experimental values simultaneously. Indeed, let us find the region where the value of magnetic moments on Fe_I atom close to experimental one, $\mu_{FeI} \approx 2.5\mu_B$. Such moment does exist in the narrow region near the line $|t_1| \approx 0.7$. But the value of the magnetic moment on Fe_{II} atom in this region is far from the experimental one, it changes within the interval $2\mu_B < \mu_{FeII}(t_1) < 3\mu_B$. And, *vice versa*, in the region where the value of moment on Fe_{II} atom is close to the experimental one $\mu_{FeII} \approx 1.5\mu_B$, the moment on the Fe_{II} atom is vanished (Fig. 3a).

Now let us switch on the NNN hoppings $t_3(Fe_{II}$-$Fe_{II})$ and $t_4(Fe_I$-$Si)$. The moment maps at the fixed values $t_3(Fe_{II}$-$Fe_{II}) = 0.4$ and $t_4(Fe_I$-$Si) = 0.7$ are shown in Fig. 3b. One can see the appearance of the region with $2\mu_B < \mu_{FeI}(t_1) < 3\mu_B$ and $1\mu_B < \mu_{FeII}(t_1) < 2\mu_B$ (see Fig. 3b), where the magnetic moments on both iron atoms can be close to experimental values simultaneously. This explicitly shows that the role played by the NNN interactions is critically essential for the formation of realistic *Fe* moments in Fe_3Si. The sensitivity of moments to $t_3(Fe_{II}$-$Fe_{II})$ is much higher than to $t_4(Fe_I$-$Si)$. Its increase makes the region of ferromagnetic state (FM) more narrow (Fig. 3b). However, the sensitivity of moments to $t_3(Fe_{II}$-$Fe_{II})$ is much higher than to $t_4(Fe_I$-$Si)$. So, the switch on the only $t_3(Fe_{II}$-$Fe_{II})$ results in the constriction of the region of FM (Fig. 3c). Especially it is pronounced for Fe_{II} atom. The moment on Fe_{II} atom is more sensitive than the one on Fe_I $\left|\frac{\partial \mu_{Fe_{II}}}{\partial t_3}\right| > \left|\frac{\partial \mu_{Fe_I}}{\partial t_3}\right|$. Besides, the NNN hopping

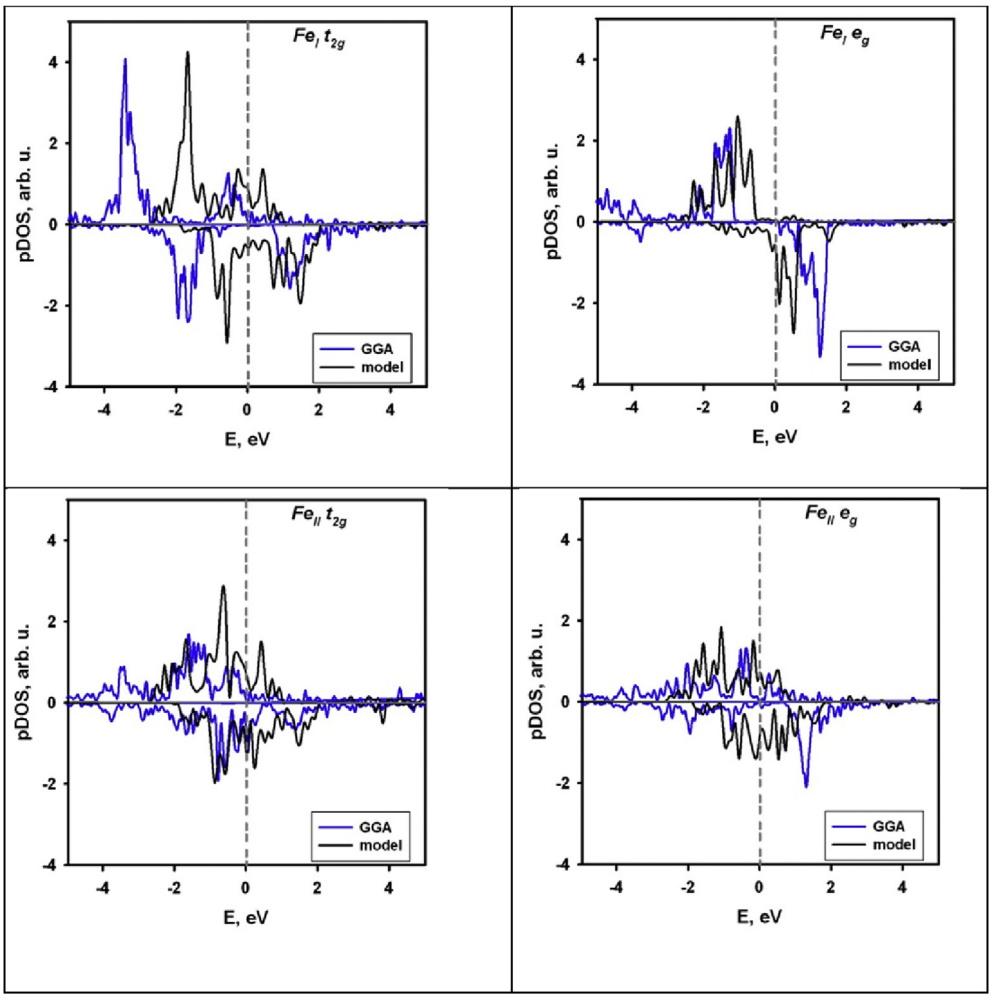

Fig. 2. Comparison of the model and GGA-DFT spin-polarized partial density of *d*-electron states. The Fermi level is taken as the zero of energy. Blue lines correspond to the GGA-DFT density of *d*-electron states and black lines are for the model ones. (For interpretation of the references to colour in this figure legend, the reader is referred to the web version of this article.)

$t_3(Fe_{II}\text{-}Fe_{II})$ is responsible for several more effects: i) the delocalization of *d*-electrons of Fe_{II}, ii) the decrease of μ_{FeII}, iii) an increase of the pDOS of *d*-electrons of Fe_{II}. The other feature of maps in Fig. 3c is the appearance of the region with ferrimagnetic state (FiM, red rectangles on the maps) of the kind $Fe_{II}\uparrow\text{-}Fe_I\downarrow$ with $|\mu_{FeI}|>|\mu_{FeII}|$ at $|t_1|>0.5$. The switching on the NNN hopping $t_4(Fe_I\text{-}Si)$ flips the moment μ_{FeII} and the region with FiM state disappears (Fig. 3b). However, it is worth noting that the FM state in Fe_3Si is stabilized by the intersite exchange interaction J'. Indeed, at $J'=0$ the FiM state is stable in all considered regions of the (t_1,t_2,t_3,t_4)-space.

In order to get a hint why the moment is so sensitive to the hopping $t_3(Fe_{II}\text{ - }Fe_{II})$, we can simplify the problem till the analytically solvable level. Namely, we replace the each many-orbital block by single-orbital one in the secular equation matrix:

$$\begin{array}{c|ccc} & Fe_I & Fe_{II} & Fe_{II} \\ Fe_I & \varepsilon_{Fe_I} & t_1(k) & t_1(k) \\ Fe_{II} & t_1(k) & \varepsilon_{Fe_{II}} & t_3(k) \\ Fe_{II} & t_1(k) & t_3(k) & \varepsilon_{Fe_{II}} \end{array} \qquad (12)$$

The eigenvalues of this matrix are

$$E_1(\boldsymbol{k}) = \varepsilon_{Fe_I} - t_3(k);$$

$$E_{2,3}(\boldsymbol{k}) = \frac{1}{2}\left[\varepsilon_{Fe_I} + \varepsilon_{Fe_{II}} \pm \sqrt{\left(\varepsilon_{Fe_I} - \varepsilon_{Fe_{II}} - t_3(k)\right)^2 + 8t_1^2(k)}\right] \qquad (13)$$

As seen, if the hopping $t_3(\boldsymbol{k})$ vanishes, the energy $E_1(\boldsymbol{k}) = \varepsilon_{Fe_I}$, i.e., becomes atomic level. Therefore, in this limit this state acquires the atomic magnetic moment. Of course, in real multi-orbital case the situation is more complex and fully atomic solution does not appear. Nevertheless, as follows from the solution of the full problem the tendency remains the same.

4. The spin-crossover

Here we consider a possibility for the crossover from the high-spin to the low-spin states under hydrostatic pressure in Fe_3Si [37,38]. DO_3 structure of Fe_3Si has two types of *Fe* positions. The Fe_I position is similar to the one in the ferromagnetic BCC-*Fe*; another iron Fe_{II} has different from the BCC-*Fe* environment. Based on the Fe_{II} pDOS shape the authors of [37] expected that such structure favors metamagnetic-like behavior under compression. The *ab initio* calculations of the total magnetic moment $\mu_{tot} = \mu_{FeI} + 2\mu_{FeII}$ of the cell of Fe_3Si under pressure have predicted the high-to low-spin crossover at the pressure P~50 *kB* [38] and P~150–200 *kB* [37]. The

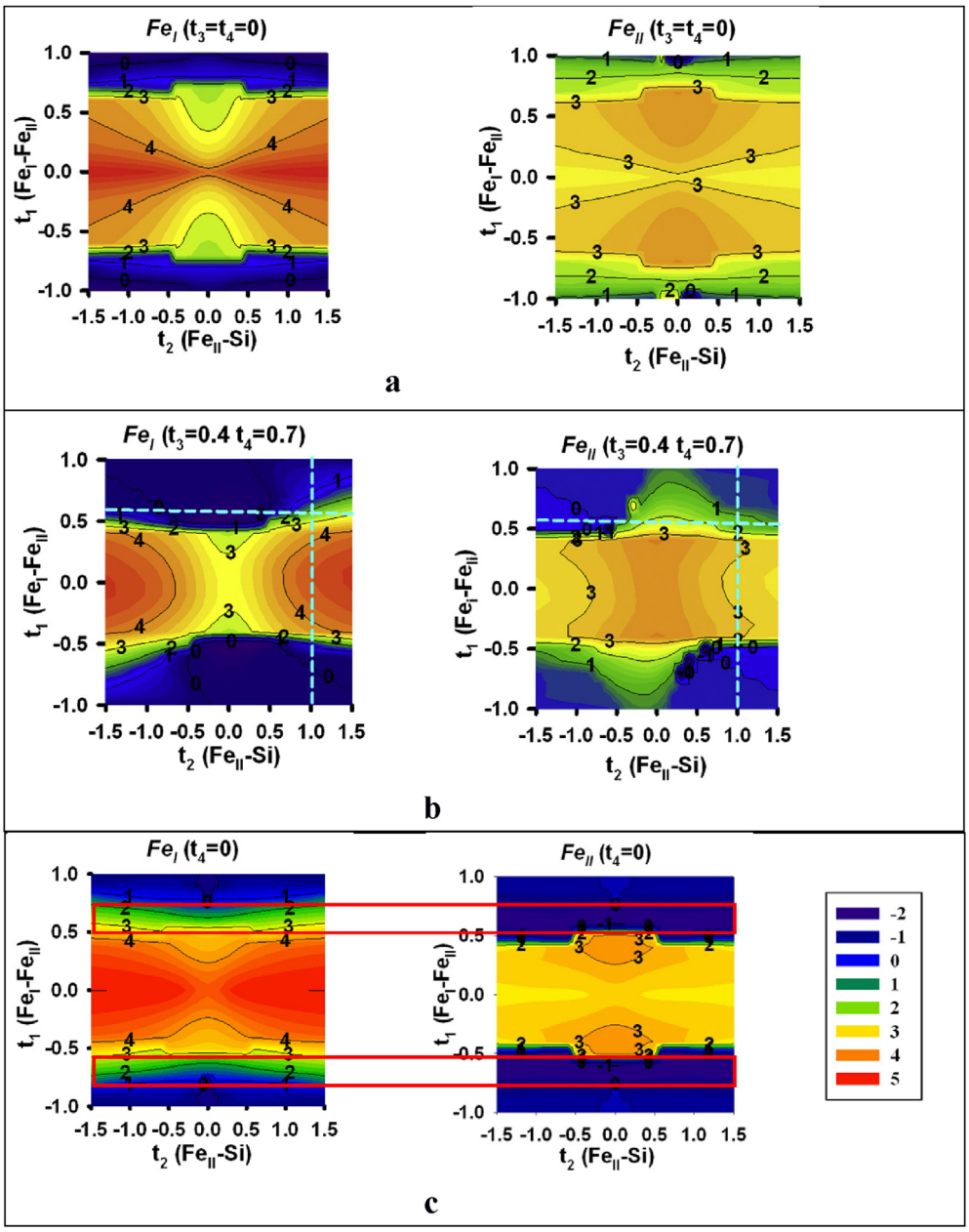

Fig. 3. The (t_1 - t_2) maps of the moments on Fe_I and Fe_{II}. a) the NNN hoppings are switched off; b) the NNN hoppings $t_3(Fe_{II}$ - $Fe_{II}) = 0.4$, $t_4(Fe_{II}$ - $Si) = 0.7$ (blue dashed lines show the parameters t_1 and t_2 from Table 1); c) only the Fe_{II} - Fe_{II} hopping t_3 is switched on. FiM areas are picked out by red rectangles. (For interpretation of the references to colour in this figure legend, the reader is referred to the web version of this article.)

calculations of the magnetic moments of two inequivalent *Fe* atoms have shown that the decrease of μ_{FeII} under pressure is responsible for the spin crossover; the μ_{FeI} almost is not dependent on the pressure.

The origin of the moments μ_{FeI}, μ_{FeII} dependence on pressure P can be understood within our model. We assume that the hopping parameters depend on a distance ΔR between the ions exponentially: $t = t_0 exp(\gamma \Delta R)$, where $t_0 = t(P = 0)$ and $\Delta R = R(P = 0)$-$R(P)$. The equilibrium lattice parameters were determined from the *ab initio* GGA calculations via minimization of the enthalpy. Then, using the values of the hopping parameters at $P = 0$ and at $P = 250$ *kB*, we obtained the following values for the parameters γ: $\gamma_1 = 0.68$ Å^{-1}; $\gamma_2 = 0.87$ Å^{-1}; $\gamma_3 = 1.31$ Å^{-1}; $\gamma_4 = 0.31$ Å^{-1} for the parameters $t_1(P)$, $t_2(P)$, $t_3(P)$, $t_4(P)$ correspondingly.

Our calculation with these parameters shows that such behavior of magnetic moments can be explained by their different dependence in the hopping matrix elements (see the upper panel of Fig. 4) on pressure.

The pressure dependences of $\mu_{FeI}(P)$ in *ab initio* and model calculations are similar to each other, $\mu_{Fe_I}(P)$ weakly decreases with pressure (see the lower panel of Fig. 4). The Fe_{II} moment behavior in model differs from one in *ab initio* calculations in the region of high pressure $P > 300$ *kB*. The $\mu^{model}_{Fe_{II}}(P)$ decreased noticeably faster than $\mu^{GGA}_{Fe_{II}}(P)$, achieving the values $\mu^{model}_{Fe_{II}}(P = 500kB) = 0.27\mu_B$ whereas $\mu^{GGA}_{Fe_{II}}(P = 500kB)$ decreased only till $0.76\mu_B$. Moreover, $\mu^{model}_{Fe_{II}}(P)$ experiences two jumps, at $P \approx 150$ *k* and $P \approx 400$ *kB*. The decrease of the magnetic moment at $P \approx 150$ *kB* is in agreement with [37],

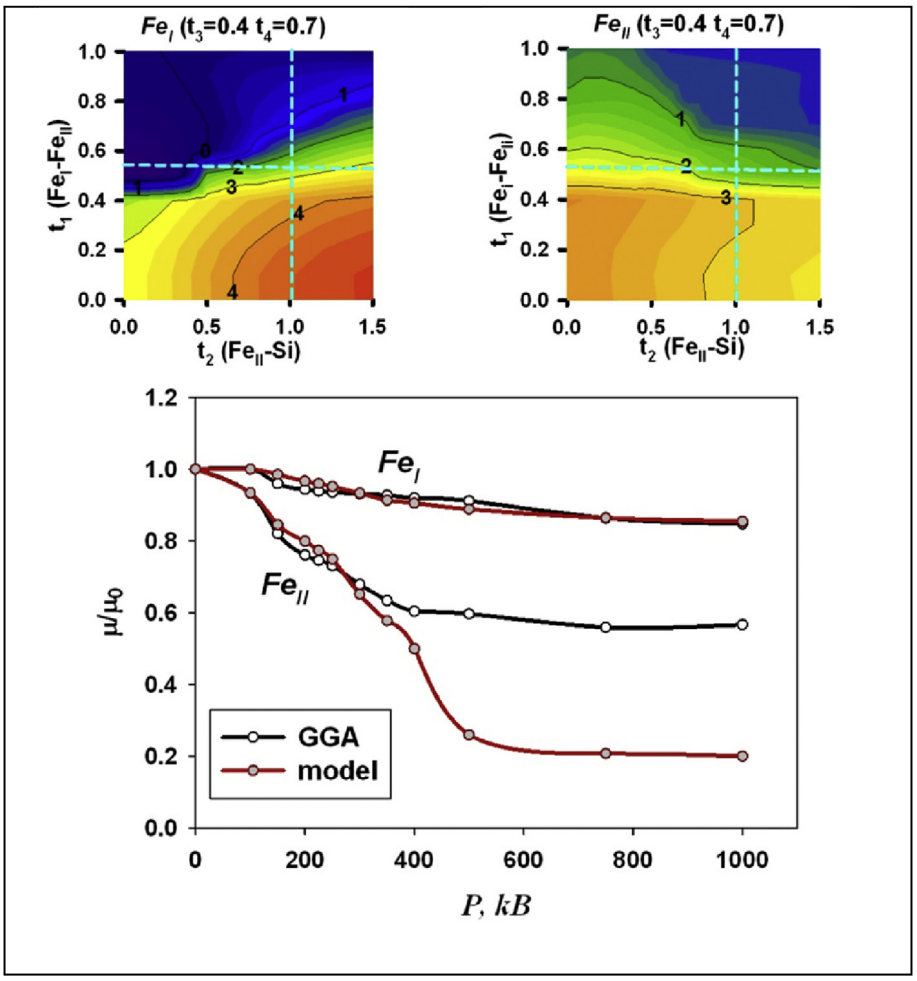

Fig. 4. Top panel: The (t_1 - t_2) maps of the moments. on Fe_I and Fe_{II}, for the positive values of NN hopping integrals (blue dashed lines show parameters t_1 and t_2 from Table 1); Bottom panel: Pressure dependence of magnetic moments; $\mu_0 = \mu(P = 0)$. (For interpretation of the references to colour in this figure legend, the reader is referred to the web version of this article.)

however, they did not consider the region of higher pressures. We are not aware of the experiments, which confirm the existence of the high-spin to low-spin crossover in *Fe₃Si*, however, it was mentioned in the work [37] that the change of the absolute reflectivity near 100 *kB* had been observed (reference [32] in Ref. [37]) in the reflectivity measurements on *Fe₃Si* and further till the pressure up to 300 *kB* no changes were found. According to our model calculations one can expect the changes in optical properties in the interval of pressure 100–200 *kB*, while the next peculiarity in moment behavior is expected at $P > 400$ *kB*.

5. The alloys Fe_xSi_{1-x}

Let us now consider the dependence of magnetic moments in alloys Fe_xSi_{1-x} on the concentration of non-magnetic *Si* atoms. The authors of [29] ascribed the changes of *Fe*-moment magnitude to an increase of the NN non-magnetic atoms number. As known, in the DO_3 structure the non-magnetic atoms prefer to occupy the positions in the Fe_I sublattice forming a partially ordered *CsCl*-like structure (B2). An increase of the *Si* concentration till 50%, i.e., when all Fe_I atoms are replaced by *Si* ones (see Fig. 5a), results in the vanishing magnetic moment of the remaining Fe_{II} atoms. The partially ordered structure of the B2 type are observed in most of epitaxial *Fe* - *Si* films [17,39]. In amorphous films situation is different: the *Si* atoms can occupy any of iron positions, Fe_I or Fe_{II}, and a chemically disordered random solid solution is formed. The electronic and magnetic properties of the epitaxial and amorphous films are also essentially different [39,40]. Particularly, the magnetic moment per iron atom in amorphous films is higher, than in epitaxial one [39,40]. For example, the experiments and *ab initio* calculations [39] show that in amorphous films the magnetic moment per *Fe* atom $\mu_{Fe} \approx 0.65\mu_B$ at 50% concentration of *Si*, contrary to the situation in the alloys with B2 structure. The main structural feature which differs disordered random solid solution from B2-like structures is the possibility of occupation of the Fe_{II} sites by *Si* atoms in the first case. This feature is directly related to the mechanisms of magnetic moment formation. As was described above, for the *Fe₃Si* the critical role in the Fe atoms moment formation is played by the presence of Fe atoms in NNN sphere. Motivated by this fact we have considered hypothetical structure (see Fig. 5b) where the additional *Si* atoms are placed into Fe_{II} sublattice. In spite of the fact that both structures shown at Fig. 5 contain the same concentration of *Si* atoms ($x = 50\%$), the *Fe* atoms moments in these structures are significantly different. This difference is caused by the different local nearest and next-nearest surrounding of Fe atoms. In first case, Fig. 5a, at 50% *Si* concentration the nearest sphere of *Fe* contains only *Si* atoms, while the next-nearest one contains only iron. In the other structure, Fig. 5b, the *Fe*

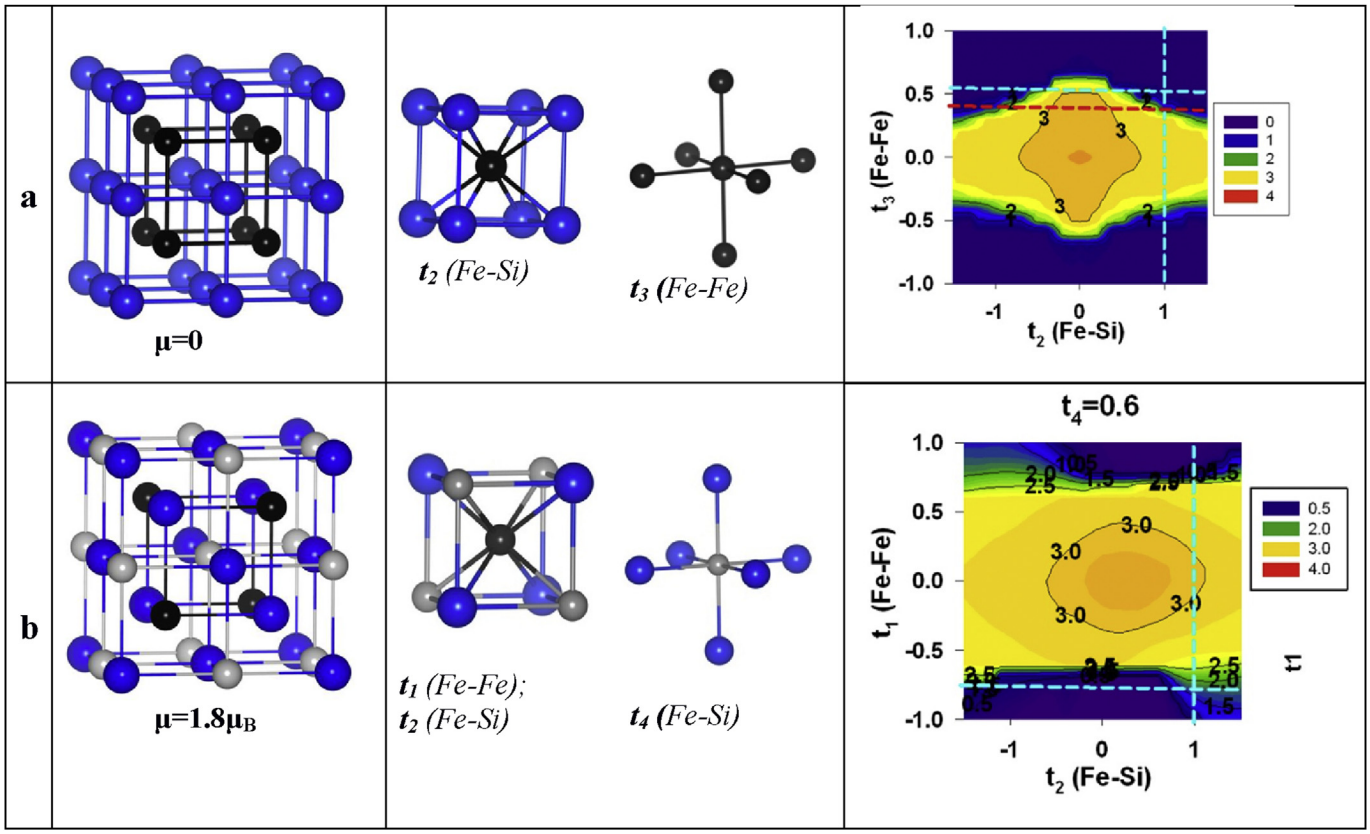

Fig. 5. Fe_xSi_{1-x} alloys ($x = 50\%$): a) *CsCl*-like structure (B2), the types of NN and NNN hoppings and *t*-maps. Red dashed line shows value of parameter $t_3 = 0.4$ (as for Fe3Si), blue dashed lines show the values of parameters $t_3 = 0.55$ and t2 = 1.0 providing the best fit of the pDOS in B2 structure; b) hypothetical structure with *Si* atoms on the Fe_{II} sites (see text), the types of NN and NNN hoppings and *t*-maps. Blue dashed lines show parameters t_1 = -0.75 and t2 = 0.9. Blue balls are *Si* atoms, grey and black balls are *Fe* atoms. (For interpretation of the references to colour in this figure legend, the reader is referred to the web version of this article.)

atoms are absent in the next-nearest sphere of *Fe*. The dependencies of *Fe* moments on the hopping constants in these two structures are shown in the last column of Fig. 5.

The red line on the magnetic moment's map in Fig. 5a shows the values of hoppings parameters $t_2 = 1.0$, $t_3 = 0.4$, corresponding to Fe_3Si case. As can be seen, they are on the border between FM and PM states in the alloy with B2 structure. A slight increase of the hopping t_3 will stabilize the PM state. Namely this mechanism works in B2 structure. The equilibrium lattice parameter for B2 structure $a(B2) = 5.52$ Å is less than one for the Fe_3Si ($a(Fe_3Si) = 5.60$ Å) and the value of hopping t_3 for B2 structure is more than one for Fe_3Si ($t_3(B2) = 0.55$, $t_3(Fe_3Si) = 0.4$). Notice that such a sharp border is characteristic for the moment maps of the *Fe* atoms which are surrounded by other *Fe* atoms (see maps in Figs. 5a and 3c). It is important that the PM state arises at NNN $t_3 \neq 0$ only. The model with NN hoppings only, even if all NN of *Fe* atoms are *Si* atoms, does not have the solutions with zero moments on *Fe*. This statement contradicts to the conclusions of earlier (much less detailed) models of local environment, where the decrease of the moment on *Fe* atoms was ascribed to the increase of number of *Si* in the nearest sphere [11,21,22].

The absence of *Fe* atoms in the next-nearest sphere (the hypothetical structure, Fig. 5b) results in the two effects: i) the equilibrium lattice parameter increases till $a = 5.71$ Å and ii) the magnetic moment $\mu_{Fe} \approx 1.8\mu_B$ arises at *Fe* atoms. The hypothetical structure (Fig. 5b) has the essential difference from the DO_3 and B2 types of structure: existence of NN *Si* - *Si* pairs at the distance $R_{Si-Si} = 2.47$ Å. So, the best model solution, corresponding to the *ab initio* calculations with $\mu_{Fe} \approx 1.8\mu_B$ arises in the model *only* at different signs of the NN hopping parameters, $t_1 = -0.75$ and $t_2 = 0.9$ (Fig. 5b, blue lines). The weak dependence of the *Fe* magnetic moment on the hopping t_2 between NN *Fe* and *Si* atoms is seen in all cases: all the t_1 - t_2-maps for *Fe* moments, calculated within this model, are elongated along the t_2 axis.

The strong dependence of the *Fe* atoms magnetic moment on the composition of next-nearest shell in the BCC type of alloys, possibly, is caused by particular spatial positions: NN atoms in BCC-like structures are arranged along the (111) direction, whereas NNN atoms are along (100). The strong σ-bond is formed from the *Fe* e_g-orbitals along (100) that delocalize e_g -electrons along this bond and, correspondingly, results in the decreasing magnetic moment.

6. Discussion and conclusions

The interpretation of the experiments [9–13] requires understanding of the role played by the local environment in the moment formation in iron silicides. This raises a question about the choice of a suitable theoretical tool for such analysis. The *ab initio* density-functional based methods allow for detailed description of the properties of compounds but it is difficult to extract from these calculations the contributions from the local environment. The many-body-theory based models allow analyzing the role played by different interactions in the formation of the material properties, as well as revealing the general for different classes of solids features. However, these two approaches use different languages. The methods, combining these two approaches, like LDA + U, LDA + DMFT, etc., contain the poorly controlled double-counting of intra-atomic interactions. The GW method requires so much of

computer resources that the problems of solids with many atoms in elementary cell become inaccessible. It is possible to translate the results obtained within DFT approach to the language of many-body theory with the help of mapping the GGA-to-DFT results to a model. In our case the choice of the model was dictated by the facts that i) the delocalized *d*-electrons are responsible for a magnetism in the materials of interest, and ii) the intratomic Coulomb interactions are the largest matrix elements for them. This lead us to the multiorbital model with the intraatomic interactions between d-electrons (similar to the Kanamori model [36]), and the *d*-*d*-intersite exchange interaction between delocalized *d*-electrons. The type the mapping, as far as we aware, have not been used before. The leading idea is as follows. The *ab initio* methods treat the strongest part of the Coulomb interactions correctly via finding the best *self-consistent* charge density, minimizing the total energy. So we choose the parameters of the model from the requirement that the model charge densities (as well as density of electron states), obtained *self-consistently*, have to be as close as possible to the GGA ones. The model is solved within the Hartree-Fock approximation (HFA). The band structure arises due to the interatomic hopping, which connect nearest neighbors (NN) and next NN (NNN) sites. The HFA calculations show that the formation of iron-atoms' moments is very sensitive to the values of namely NNN hopping parameters. This statement has been demonstrated by comparison of the moment formation maps with and without NNN hopping parameters. The characteristic feature of these maps is the presence of the parameter regions with very fast change of the magnetic moments as a function of hopping between two types of iron (Fe_I - Fe_{II}). The NNN hopping (Fe_{II} - Fe_{II}) makes the ferromagnetic (FM) region narrower and at large enough value results in the transition into ferrimagnetic state. Notice that the Stoner's like criteria for FM instability, which is natural for the models with delocalized electrons, is not sufficient here. Indeed, speculating from the strong-coupling-side perturbation theory (SCPT) the Hubbard-model-like effective antiferromagnetic interaction $-t^2/U$ forms the ferrimagnetic state (FiM; the state with oppositely directed but modulo different moments on inequivalent *Fe* atoms). So, the stabilizing FM state direct *Fe*-*Fe* exchange interaction should be strong enough to overcome the AFM-like contributions. In order to make mapping we have used the weak-coupling theory (WCPT). However, the WCPT HFA captures the effects of SCPT the better the stronger is an orbital polarization. So, as seen from solutions, WCPT HFA is capable to take into account AFM interactions.

It may be looked that the presented analysis is of theoretical interest only. However, the hopping parameters are the most sensitive parameters to different type of pressure. This statement follows from the fitting the hopping parameters of the model within the same scheme to the results of *ab initio* calculation of the enthalpy for Fe_3Si at different pressures. The pressure can be made negative, either chemically or by depositing the films on the substrate with larger than the iron silicide lattice parameter; or positive, by applying the hydrostatic pressure or depositing the films on the substrate with smaller lattice parameter.

The effect of the high-spin to low-spin crossover is predicted by both GGA and model calculations. Namely, the moment of Fe_{II} atom sharply decreases whereas the moment of Fe_I remains almost intact. The model calculation predicts also second crossover at higher pressure. It worth noting that here the spin-crossover arises not due to the standard mechanism of competition between the crystal-field splitting and *d*-*d* Hund exchange interaction, but is caused mainly by the delocalization of *d*-electrons.

At last, we have considered the mechanisms of moment formation in solid solutions Fe_xSi_{1-x}. Theoretically such alloys usually are studied within the coherent-potential approximation (CPA). By calculation of several hypothetical structures we explicitly show that *at the same concentration different magnetic structures arise* due to different NN and NNN environments for *Fe* atoms, the statement which is beyond reach of the CPA. Particularly, this finding allows also explaining the difference in the properties partially ordered alloys with B2 structures and the amorphous alloys.

Thus, we can conclude that the decisive role in the formation of *Fe* atoms magnetic moments is played by the effects of local environment in spite of the delocalized nature of d-electrons in the iron silicides. The contribution of NNN hopping to it is quite significant. The existence of the region with sharp transition from ferro-to paramagnetic state as well as the predicted spin crossovers strongly improve the perspectives of the practical applications of iron silicide films and, hopefully, will stimulate technologists to find a way to make the films near the instability line with desirable characteristics.

Acknowledgement

This work was supported by the Grants of Russian Foundation for Basic Research № 14-02-00186, № 17-02-00161 and by the Grants of Russian Foundation for Basic Research and Government of Krasnoyarsk Territory № 16-42-243035, 16-42-242036. The authors would like to thank AS Shinkorenko for the technical support.

References

[1] Y. Maeda, T. Jonishi, K. Narumi, Y. Ando, K. Ueda, M. Kumano, T. Sadoh, M. Miyao, Appl. Phys. Lett. 91 (2007) 171910.
[2] J. Kudrnovsky, N.E. Christensen, O.K. Andersen, Phys. Rev. B 43 (1991) 5924.
[3] A. Bansil, S. Kaprzyk, P.E. Mijnarends, J. Tobola, Phys. Rev. B 60 (1999) 13396.
[4] K. Hamaya, K. Ueda, Y. Kishi, Y. Ando, T. Sadoh, M. Miyao, Appl. Phys. Lett. 93 (2008) 132117.
[5] K. Hamaya, T. Murakami, S. Yamada, K. Mibu, M. Miyao, Phys. Rev. B 83 (2011) 144411.
[6] O. Kubaschewski, Iron-binary Phase Diagrams, Springer-Verlag, New York, 1982.
[7] G. Bertotti, A.R. Ferchmin, E. Fiorillo, K. Fukamichi, K. Kobe, S. Roth, Magnetic Allows for Technical Applications. Soft Magnetic Allows. Invar and Elinvar Allows (Landolt Bornstein, New Series vol.III/19il), Springer, Berlin, 1994, 33–142.
[8] V.A. Niculescu, T.J. Burch, J.I. Budnick, JMMM 39 (1983) 223–267.
[9] S. Yoon, J.G. Booth, Phys. Rev. Lett. 48A (1974) 381.
[10] A. Paoletti, L. Passari, Nuovo Cimento 32 (1964) 25.
[11] A.K. Arzhnikov, L.V. Dobysheva, E.P. Yelsukov, G.N. Konygin, E.V. Voronina, Phys. Rev. B 65 (2002) 024419.
[12] T.J. Burch, T. Litrenta, J.I. Budnick, Phys. Rev. Lett. 33 (1974) 421.
[13] M.B. Stearns, Phys. Rev. B 4 (1971) 4069.
[14] D. Berling, G. Gewinner, M.C. Hanf, K. Hricovini, S. Hong, et al., JMMM 191 (1999) 331.
[15] A. Ionescu, C.A. Vaz, T. Trypiniotis, C.M. Curtler, H. Garsia-Miquel, J.A.C. Bland, Phys. Rev. B 71 (2005) 094401.
[16] M. Walterfang, W. Keune, K. Trounov, R. Peters, U. Ruecker, K. Westerholt, Phys. Rev. B 73 (2006) 214423.
[17] A.X. Gray, J. Karel, J. Miñar, C. Bordel, et al., Phys. Rev. B 83 (2011) 195112.
[18] I.A. Yakovlev, S.N. Varnakov, B.A. Belyaev, et al., JETP Lett. 99 (9) (2014) 527–530.
[19] S.A. Lyaschenko, Z.I. Popov, S.N. Varnakov, et al., JETP 120 (5) (2015) 886–893.
[20] Guixin Cao, D.J. Singh, X.-G. Zhang, et al., Phys. Rev. Lett. 114 (2015) 147202.
[21] W.A. Hines, A.H. Menotti, J.I. Budnick, T.J. Burch, T. Litrenta, V. Niculescu, K. Ray, Phys. Rev. B 13 (1976) 4060.
[22] E.P. Elsukov, G.N. Konygin, V.A. Barinov, E.V. Voronina, J. Phys. Condens. Matter 4 (1992) 7597.
[23] J. Kudrnovsky, N.E. Christensen, O.K. Andersen, Phys. Rev. B 43 (1990) 5924.
[24] T. Khmelevska, S. Khmelevskyi, A.V. Ruban, P. Mohn, J. Phys. Condens. Matter 18 (2006) 6677.
[25] N.I. Kulikov, D. Fristol, J. Hugel, A.V. Postnikov, Phys. Rev. B 66 (2002) 014206.
[26] A. Bansil, S. Kaprzyk, P.E. Mijnsrends, J. Tobola, Phys. Rev. B 60 (1999) 13396.
[27] A. Go, M. Pugaczowa-Michalska, L. Dobrzyński, Eur. Phys. J. B 59 (2007) 1.
[28] E. Voronina, et al., Nucl. Instrum. Methods Phys. Res. A 575 (2007) 189.
[29] A.K. Arzhnikov, L.V. Dobysheva, Itinerant Electron Magnetism: Fluctuation Effects Volume 55 of the Series NATO Science Series, 1998, pp. 375–389.
[30] E.J. Garba, R.L. Jacobs, J. Phys. F Metal Phys. 16 (1986) 1485.
[31] J.C. Slater, G.F. Koster, Phys. Rev. 94 (1954) 1498.
[32] G. Kresse, J. Furthmuller, Comput. Mat. Sci. 6 (15) (1996). G.Kresse and J. Furthmuller Phys. Rev. B 54 11169(1996).
[33] P.E. Blochl, Phys. Rev. B 50 (1994) 17953. G.Kresse and D.Joubert Phys. Rev. B 59, 1758 (1999).

[34] J.P. Perdew, K. Burke, M. Ernzerhof, Phys. Rev. Lett. 77 (1996) 3865. J.P.Perdew, K.Burke and M.Ernzerhof Phys. Rev. Lett. 78, 1396(1997).
[35] H.J. Monkhorst, J.D. Pack, Phys. Rev. B 13 (1976) 5188.
[36] J. Kanamori, Prog. Theor. Phys. 30 (1963) 275.
[37] N.E. Christensen, J. Kudrnovsky, C.O. Rodrigues, Int. J. Mater. Sci. Simul. 1 (2007) 1.
[38] Joo Yull Rhee, B.N. Harmon, Phys. Rev. B 70 (2004) 094411.
[39] J. Karel, J. Juraszek, C. Minar, K. Bordel, et al., Phys. Rev. B 91 (2015) 144402.
[40] J. Karel, Y.N. Zhang, C. Bordel, K.H. Stone, et al., Mater. Res. Express 1 (2014) 026102.